water

MDPI

Article

Pressure-Flow Scour under a Bridge Deck in Clear Water Conditions

Fahmy Salah Abdelhaleem [1], Ibrahim M. Mohamed [2], Ibrahim G. Shaaban [3,*], Atiyeh Ardakanian [3], Wael Fahmy [2] and Amir Ibrahim [1]

[1] Civil Engineering Department, Benha Faculty of Engineering, Benha University, Benha 13512, Egypt
[2] Civil Engineering Department, Shoubra Faculty of Engineering, Benha University, Shoubra 11629, Egypt
[3] Civil Engineering Department, School of Computing and Engineering, University of West London, London W5 5RF, UK
* Correspondence: ibrahim.shaaban@uwl.ac.uk

Abstract: The issues of scouring around a bridge have become prominent in recent research mainly due to recurrent extreme weather events. Thus, designing a bridge with the appropriate protection measures is essential to safeguard it against failure, which may take place due to scouring from high flows resulting from extreme weather events. Bridges may become partially or entirely submerged during extreme weather events such as large floods and are subject to pressure-flow scour, a condition where the flow is directed downward and under the bridge deck, creating an increase in flow velocity and a corresponding increase in bed scour. This study aims to explore the pressure-flow scour depth under a bridge deck without piers in the presence of two vertical wall abutments under clear water experiments. Sixty-six tests were conducted involving the approach flow depth, bed material size, contraction length, contraction width, and bridge opening for both pressure and free surface flow conditions. An empirical equation was deduced to determine the maximum scour depth, which could be applied as a preliminary design for bridges under pressure-flow conditions. The experimental data were used to determine the performance of the earlier models of pressure-flow scour. The results revealed that for pressure-flow conditions, the maximum scour depth increased by a factor between 2.15 and 9.81 times the maximum scour depth under free surface flow conditions. With same flow depth, when the relative bridge length was increased from 5 to 7.5 and 7.5 to 10, the maximum scour depth decreased by up to about 7.4% and 2.3%, respectively. When the relative bridge width was decreased from 5.5 to 5.2 and 5.2 to 4.4, the maximum scour depth increased by up to about 45.6% and 81.2%, respectively.

Keywords: bridge abutments; clear water scour; free flow; local scour; pressure flow; pressure scour

Citation: Abdelhaleem, F.S.; Mohamed, I.M.; Shaaban, I.G.; Ardakanian, A.; Fahmy, W.; Ibrahim, A. Pressure-Flow Scour under a Bridge Deck in Clear Water Conditions. *Water* **2023**, *15*, 404. https://doi.org/10.3390/w15030404

Academic Editor: Maria Mimikou

Received: 22 December 2022
Revised: 9 January 2023
Accepted: 13 January 2023
Published: 18 January 2023

1. Introduction

Local scours at bridges are among the most common reasons for bridge failure [1]. The waterway at a bridge site may contract horizontally because of the presence of bridge abutments or bridge piers and/or vertically when a bridge deck gets submerged. Clear water scouring due to flow area contraction at the bridge site occurs because the corresponding flow velocity at the contraction increases as the cross-section area decreases. This increase in flow velocity produces additional bed shear stress, resulting in the transportation of bed materials out of the area of contraction until the maximum scour occurs when the flow velocity is equal to the critical velocity, or the bed shear stress is equal to the critical shear stress in the contraction area [2]. Pressure-flow (vertical contraction) scour occurs during floods or when a bridge deck is not high enough such that when the water surface exceeds the lower elevation of the superstructure elements of the bridge, the bridge deck and/or girder becomes a barrier to the flow. A bridge deck is considered partially submerged (pressure flow) when the flowing water reaches the lowest element

of the bridge. As the water level increases, the pressurized flow under the bridge increases as the degree of submergence increases. However, when the flowing water passes over the bridge, the flow is considered fully submerged (combined weir overflow) [3,4].

Most published studies have paid attention to free surface flow scours [5,6]. Meanwhile, pressure-flow scours have received less attention [7]. Abed [8] introduced the first study on pressure-flow pier scour at a bridge with piers. She deduced experimental equations for predicting the pressure-flow scour depth at a bridge pier based on 25 experiments governed by clear water scour conditions. In such studies, differentiating between the pressure-flow scour and the pier scour was difficult as all experiments comprised both a bridge deck and a pier model. Arneson and Abt [9] developed a laboratory formula to estimate the scour hole due to the pressure flow beneath a bridge deck. This equation is also employed in HEC-18 to determine the scour depth under pressure flow conditions (see Table 1). Umbrell et al. [3] experimentally studied a scour under a bridge deck without abutments and piers under pressure flow conditions. They analyzed their experimental results by applying the continuity equation of flow passing under and over the bridge's deck. Lyn [4] evaluated the HEC-18 equation for estimating pressure-flow scour. He reported that the experimental time to attain the equilibrium scour depth of the data sets of Arneson [10] and Umbrell et al. [3] might be insufficient. He also reanalyzed those data and developed a design equation (see Table 1). Guo et al. [11] deduced an analytical solution based on the energy and mass conservation laws for pressure-flow scour. Their theoretical solution can predict the maximum pressure-flow scour and a corresponding scour profile. Lin et al. [12] employed particle image velocimetry and flow visualization techniques to explore the flow structure under a partially submerged deck. According to the Froude number and submergence ratios, they defined four types of flow structures beneath the deck. Shan et al. [13] performed an analytical and experimental study to propose an equation for the maximum pressure-flow scour depth. They combined their experimental data with the data sets of Arneson and Abt [9] and Umbrell et al. [3] to deduce a design model. They also agreed with Lyn [4] that the pressure-flow scour at highway bridges required an improved model. Dankoo et al. [14] experimentally developed a formula to estimate the amount of scour at bridge piers in compound channels with vegetation under pressurized flow conditions. Kocyigit and Karakurt [15] experimentally investigated the pressure flow and combined weir overflow at bridge decks under clear water conditions. They considered the approach flow depths, girder depths, bed materials, and degrees of submergences and developed two equations for pressure flow and combined weir overflow to predict the maximum depth of scour (see Table 1). They reported that new experiments are required to fill a gap in the available literature.

A review of the available literature on pressure-flow scour at bridges revealed that experiments on a wider range of parameters are needed [15]. Most recent studies have not explored the direct effect of the median particle diameter of bed materials [7]. Likewise, the effects of bridge length (length of contraction) and the aspect ratio of the channel (bridge width to channel width) on the scour depth have not been reported in any study. This study aims to experimentally explore the maximum scour depth at a bridge deck with two girders and without piers under pressure flow governed by clear water conditions in the presence of two vertical wall abutments. The effects of bridge length and the aspect ratio of the channel on the pressure-flow scour were tested. A total of 66 laboratory tests were performed: 55 runs for pressure-flow conditions (partially submerged) and 11 runs for the free surface flow conditions (atmospheric flow). The approach flow depth, bed material size, bridge length, bridge width, and submergence ratios (relative bridge openings) were studied for both flow conditions.

Table 1. Prediction equations for the pressure-flow scours.

Model/ Equation	Remarks
Arneson and Abt [9] $\frac{y_s}{y_a} = -5.08 + 1.27\frac{y_a}{y_b} + 4.44\frac{y_b}{y_a} + 0.19\frac{V_a}{V_c}$	V_c = critical velocity $V_c = C\sqrt{g(S_g - 1)d_{50}}(y_a/d_{50})^{1/6}$ C = 1.52
Umbrell et al. [3] $\frac{y_s + y_b}{y_a} = 1.102\left[\frac{V_a}{V_c}\left(1 - \frac{w}{y_a}\right)\right]^{0.603} + 0.06$	w = flow depth overtopping bridge C = 1.58 in critical velocity, V_c equation
Lyn [4] $\frac{y_s}{y_a} = min\left[0.21\left(\frac{V_b}{V_c}\right)^{2.95}, 0.6\right]$	
Guo et al. [11] $y_s = (y_b + h)\sqrt{\frac{1 + \frac{\lambda}{F_i^m}}{1 + \frac{2\beta}{F_i^2}}} - y_b$	$h = y_a - y_b = (h_s + h_g)$ F_i = inundation Froude number $F_i = \frac{V_a}{\sqrt{g(y_a - y_b)}}$ λ, m, β = constanta parameters
HEC-18 Equation [2] $y_s = y_2 + t - y_b$ $y_2 = \left[\frac{K_u Q^2}{d_m^{2/3} B}\right]^{3/7}$ $t = 0.5\left[\frac{y_b.(h_g + h_s)}{y_a^2}\right]^{0.20}.y_b$	K_u = 0.0077 (English units) Q = flow discharge (ft³/s) d_m = diameter of the smallest non-transportable particle in the bed material (= *1.25.*d_{50}) h_g = girder depth
Shan et al. [13] $y_s = \left[\frac{V_a(y_a - w)}{K_u\, d_{50}^{1/3}}\right]^{6/7} + \left[0.5\left(\frac{y_b y_a}{y_a^2}\right)^{0.2}\left(1 - \frac{w}{y_a}\right)^{-0.1} - 1\right]y_b$	K_u = constant = 6.17 m²/s
Melville [16] $\frac{y_s}{y_a} = 0.75\left(\frac{V_a}{V_c} - 0.4\right), \quad 0.4 < \frac{V_a}{V_c} \le 1$ $\frac{y_s}{y_a} = 0.45, \quad 1 < \frac{V_a}{V_c} \le 2.5$	
Kumcu [17] $\frac{y_s + y_b}{y_a} = 0.65 + 0.5\frac{V_b}{V_c}, \quad 0.5 \le \frac{V_b}{V_c} < 1$ $\frac{y_s + y_b}{y_a} = 1.025 + 0.125\frac{V_b}{V_c}, \quad 1 \le \frac{V_b}{V_c} \le 1.8$	
Kocyigit and Karakurt [15] $\frac{y_s}{y_b} = -0.962 - 0.187\frac{y_a}{y_b} + 0.443F_b^* + 0.672\frac{h_g}{y_b}$	h_g = girder depth F_b^* = densimetric Froude number of the flow passing under the bridge deck $F_b^* = \frac{V_b}{\sqrt{g(S_g - 1)d_{50}}}$

2. Materials and Methods

2.1. Experimental Setup

All experiments were accomplished in a 17.6 m long, 0.60 m wide, and 0.60 m deep recirculating flume with a steel horizontal bed and glass walls in the hydraulic laboratory of the Faculty of Engineering, Menoufia University, Egypt. A tailgate was located at the downstream end of the flume to adjust the selected approach flow depth. An ultrasonic flowmeter installed on the feeding pipe with a reading accuracy of ± 1.0% was used to measure the flow rate. Point gauges with an accuracy of ± 0.1 mm, were employed to determine the flow depth and bed levels. Moreover, the flow velocity was measured using

a SonTek acoustic Doppler velocimeter (San Diego) with a side-looking 3D probe. A sampling rate of 200 Hz was used to measure the water velocity profiles. The model of the bridge deck was adjustable in the experiments to be perpendicular to the direction of flow and measured 0.50 m long, 0.60 m wide, and 0.25 m deep based on a two-lane bridge scaled at 1 to 100. Two girders beneath the bridge deck, 1.50 cm high and 0.80 cm wide, were used and kept constant in all tests. Two wood pieces, 2.5 cm wide and 0.50 m long, were glued to the flume as vertical wall abutments from both sides. Three piezometric tubes were installed on the bridge deck to observe the pressure head along the bridge deck (Figure 1). The chosen coordinate system had an origin at the surface of the bed level on the centerline of the working section where the bridge deck begins. The horizontal coordinates, x and y, are nondimensionalized by the length of the bridge in the longitudinal direction.

A working section 8.0 m long, 0.60 m wide, and 0.30 m deep was placed 6.0 m downstream of the flume inlet and filled with a 0.30 m-thick layer of sand as bed material. Three different sizes of sand with median diameters of d_{50} = 1.093, 1.469, and 2.575 mm were employed to examine the bed material size effect on the scour depth under pressure flow. The geometric standard deviations (σ_g) for the three bed material samples were 1.302, 1.198, and 1.274, the uniformity coefficients (C_u) were 1.611, 1.292, and 1.612, and the curvature coefficients (C_c) were 0.937, 0.951, and 0.983, respectively. The dry bed materials' angle of repose was about 31°, and the specific gravity of the bed materials was S_g = 2.65. The tested bed materials are uniform because $\sigma_g < 1.4$, $C_u < 3.0$, and $C_c < 1.5$ [15, 18]. The armoring effect would not occur in this study as $\sigma_g < 1.3$ [19,20].

A flume discharge of 18 l/s with five approach flow depths of y_a = 8, 9, 10, 12, and 15 cm was tested. The tests were conducted in a semi-uniform flow. A clear water condition was attained in all experiments as the approach velocity (Va) to the computed critical velocity (V_c) obtained using Neill's [21] equation, $V_c = 1.52\sqrt{g(S_g - 1)d_{50}}(y_a/d_{50})^{1/6}$, is less than one ($V_a/V_c < 1$) [15, 22]. In this study, the computed V_a/V_c varied between 0.436 and 0.907. The experiments were executed at five different degrees of submergence for pressure-flow conditions and one case for the free surface flow condition. Three bridge lengths were considered (L = 50, 75, and 100 cm), and three bridge widths were tested (b_{br} = 55, 52, and 44 cm). Table 2 represents the values of the tested parameters in these experiments, The model of the bridge deck was installed at the middle of the working section, at 10.0 m downstream of the flume inlet where the boundary layer is fully developed (Figure 2). Guo et al. [23] and Shan et al. [13] defined the equilibrium time for the scour depth for three continuous hours, and the changes in scour at a reference point were less than 1 mm. In this study, preliminary runs showed that 10 h of test duration was adequate to attain the equilibrium condition.

For each run, bed materials in the working section were leveled. Water was released to the flume gradually from the downstream end until the flow depth was greater than the tested flow depth. Then, the pump was switched on such that the bed materials would not be disturbed or transported. Thereafter, the discharge was measured. When the flow discharge was adjusted, the considered water depth was adapted employing the tailgate. Then, the deck was slowly slid to the model. The flow discharge and depth were checked again, and the test began. For each run, the piezometric tube was used to observe the pressure head along the bridge deck. Flow depths were determined using the point gauges. Five vertical velocity profiles were measured along the centerline of the test section. At the end of the test, the pump was switched off and the water was drained very slowly; then, the deck was removed from the flume. The bed elevations were surveyed using the point gauges to define the scour profiles and determine the maximum scour depth. The experimental data for the pressure and atmospheric flows are summarized in Table 3.

(**a**)

(**b**)

Figure 1. Experimental apparatus: (**a**) bridge deck and vertical wall abutments; (**b**) elevation and side view.

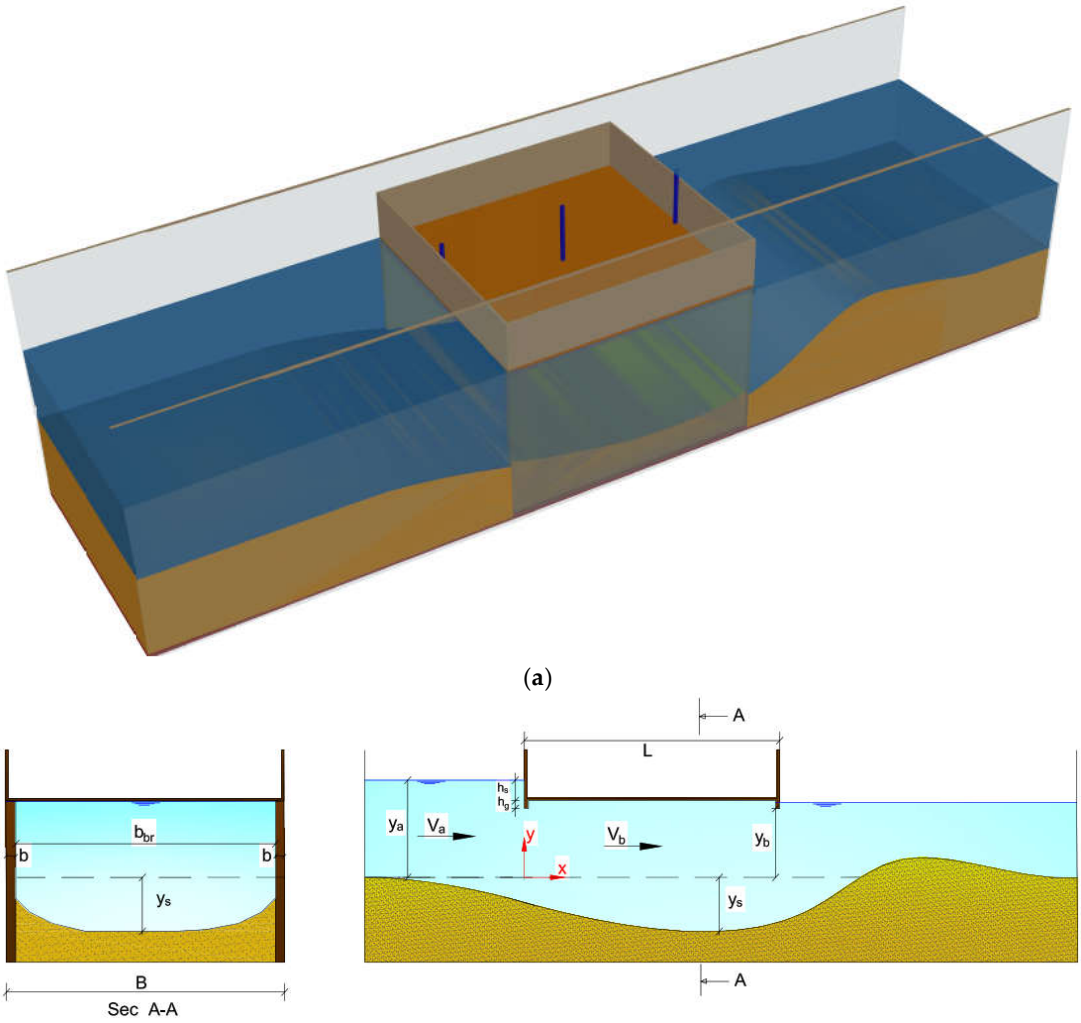

Figure 2. Definition diagram for tested apparatus: (**a**) 3D view; (**b**) side view and sec A-A.

Table 2. Values of experimental parameters.

Parameter	Values
Approach flow depth, y_a	8, 9, 10, 12, and 15 cm
Girder dimension	1.5 cm height and 0.8 cm width
Bridge length, L	50, 75, and 100 cm
Bridge width, b_{br}	55, 52, and 44 cm
Median diameter, d_{50}	1.093, 1.469, and 2.575 mm
Geometric standard deviations, σ_g	1.302, 1.198, and 1.274

Table 3. Laboratory data and computed scour number.

Test	y_a (cm)	y_b (c)	L (cm)	b_{br} (cm)	h_s (cm)	V_a (m/s)	d_{50} (mm)	σ_g (-)	F_a (-)	F_a^* (-)	y_s (cm)	Scour number
1	15.0	6.00	50	55	7.50	0.200	1.093	1.302	0.165	0.128	8.22	0.948
2	15.0	9.00	50	55	4.50	0.200	1.093	1.302	0.165	0.128	5.86	0.990
3	15.0	10.50	50	55	3.0	0.200	1.093	1.302	0.165	0.128	2.49	0.866
4	15.0	12.00	50	55	1.5	0.200	1.093	1.302	0.165	0.128	0.42	0.828
5	15.0	12.75	50	55	0.8	0.200	1.093	1.302	0.165	0.128	0.45	0.880

6	12.0	4.50	50	55	6.0	0.250	1.093	1.302	0.230	0.179	9.73	1.186
7	12.0	6.90	50	55	3.6	0.250	1.093	1.302	0.230	0.179	7.51	1.201
8	12.0	8.10	50	55	2.4	0.250	1.093	1.302	0.230	0.179	5.58	1.140
9	12.0	9.30	50	55	1.2	0.250	1.093	1.302	0.230	0.179	4.01	1.109
10	12.0	9.90	50	55	0.6	0.250	1.093	1.302	0.230	0.179	2.14	1.003
11	10.0	3.50	50	55	5.0	0.300	1.093	1.302	0.303	0.236	10.39	1.389
12	10.0	5.50	50	55	3.0	0.300	1.093	1.302	0.303	0.236	9.27	1.477
13	10.0	6.50	50	55	2.0	0.300	1.093	1.302	0.303	0.236	8.17	1.467
14	10.0	7.50	50	55	1.0	0.300	1.093	1.302	0.303	0.236	6.120	1.362
15	10.0	8.00	50	55	0.5	0.300	1.093	1.302	0.303	0.236	4.69	1.270
16	9.00	3.00	50	55	4.5	0.333	1.093	1.302	0.355	0.276	11.62	1.624
17	9.00	4.80	50	55	2.7	0.333	1.093	1.302	0.355	0.276	10.44	1.693
18	9.00	5.70	50	55	1.8	0.333	1.093	1.302	0.355	0.276	9.26	1.662
19	9.00	6.60	50	55	0.9	0.333	1.093	1.302	0.355	0.276	8.03	1.625
20	9.00	7.05	50	55	0.5	0.333	1.093	1.302	0.355	0.276	6.51	1.507
21	8.00	2.50	50	55	4.0	0.375	1.093	1.302	0.423	0.330	13.13	1.954
22	8.00	4.10	50	55	2.4	0.375	1.093	1.302	0.423	0.330	10.73	1.854
23	8.00	4.90	50	55	1.6	0.375	1.093	1.302	0.423	0.330	9.76	1.832
24	8.00	5.70	50	55	0.8	0.375	1.093	1.302	0.423	0.330	9.23	1.866
25	8.00	6.10	50	55	0.4	0.375	1.093	1.302	0.423	0.330	9.08	1.897
26	10.0	3.50	50	55	5.0	0.300	1.469	1.198	0.303	0.236	9.12	1.262
27	10.0	5.50	50	55	3.0	0.300	1.469	1.198	0.303	0.236	8.13	1.363
28	10.0	6.50	50	55	2.0	0.300	1.469	1.198	0.303	0.236	7.14	1.364
29	10.0	7.50	50	55	1.0	0.300	1.469	1.198	0.303	0.236	5.36	1.286
30	10.0	8.00	50	55	0.5	0.300	1.469	1.198	0.303	0.236	4.09	1.209
31	10.0	3.50	50	55	5.0	0.300	2.575	1.274	0.303	0.236	8.78	1.228
32	10.0	5.50	50	55	3.0	0.300	2.575	1.274	0.303	0.236	7.83	1.333
33	10.0	6.50	50	55	2.0	0.300	2.575	1.274	0.303	0.236	6.69	1.320
34	10.0	7.50	50	55	1.0	0.300	2.575	1.274	0.303	0.236	5.09	1.259
35	10.0	8.00	50	55	0.5	0.300	2.575	1.274	0.303	0.236	3.81	1.181
36	10.0	3.50	75	55	5.0	0.300	1.093	1.302	0.303	0.236	9.77	1.327
37	10.0	5.50	75	55	3.0	0.300	1.093	1.302	0.303	0.236	8.81	1.431
38	10.0	6.50	75	55	2.0	0.300	1.093	1.302	0.303	0.236	7.51	1.401
39	10.0	7.50	75	55	1.0	0.300	1.093	1.302	0.303	0.236	5.45	1.295
40	10.0	8.00	75	55	0.5	0.300	1.093	1.302	0.303	0.236	4.37	1.237
41	10.0	3.50	100	55	5.0	0.300	1.093	1.302	0.303	0.236	9.46	1.296
42	10.0	5.50	100	55	3.0	0.300	1.093	1.302	0.303	0.236	8.53	1.403
43	10.0	6.50	100	55	2.0	0.300	1.093	1.302	0.303	0.236	7.19	1.369
44	10.0	7.50	100	55	1.0	0.300	1.093	1.302	0.303	0.236	5.57	1.307
45	10.0	8.00	100	55	0.5	0.300	1.093	1.302	0.303	0.236	4.23	1.223
46	10.0	3.50	50	52	5.0	0.300	1.093	1.302	0.303	0.236	16.00	1.950
47	10.0	5.50	50	52	3.0	0.300	1.093	1.302	0.303	0.236	12.98	1.848
48	10.0	6.50	50	52	2.0	0.300	1.093	1.302	0.303	0.236	12.58	1.908
49	10.0	7.50	50	52	1.0	0.300	1.093	1.302	0.303	0.236	8.57	1.607
50	10.0	8.00	50	52	0.5	0.300	1.093	1.302	0.303	0.236	6.58	1.458
51	10.0	3.50	50	44	5.0	0.300	1.093	1.302	0.303	0.236	27.12	3.062
52	10.0	5.50	50	44	3.0	0.300	1.093	1.302	0.303	0.236	24.60	3.010
53	10.0	6.50	50	44	2.0	0.300	1.093	1.302	0.303	0.236	21.49	2.799
54	10.0	7.50	50	44	1.0	0.300	1.093	1.302	0.303	0.236	15.98	2.348
55	10.0	8.00	50	44	0.5	0.300	1.093	1.302	0.303	0.236	12.47	2.047
56	15.0	15.00	50	55	0.0	0.200	1.093	1.302	0.165	0.128	0.41	1.028

57	12.0	12.00	50	55	0.0	0.250	1.093	1.302	0.230	0.179	0.51	1.043
58	10.0	10.00	50	55	0.0	0.300	1.093	1.302	0.303	0.236	3.30	1.330
59	9.00	9.00	50	55	0.0	0.333	1.093	1.302	0.355	0.276	3.34	1.371
60	8.00	8.00	50	55	0.0	0.375	1.093	1.302	0.423	0.330	3.74	1.467
62	10.0	10.00	50	55	0.0	0.300	1.469	1.198	0.303	0.236	1.81	1.861
63	10.0	10.00	50	55	0.0	0.300	2.575	1.274	0.303	0.236	0.73	1.181
64	10.0	10.00	75	55	0.0	0.300	1.093	1.302	0.303	0.236	3.14	1.073
65	10.0	10.00	100	55	0.0	0.300	1.093	1.302	0.303	0.236	3.00	1.314
66	10.0	10.00	50	52	0.0	0.300	1.093	1.302	0.303	0.236	4.62	1.300

2.2. Dimensional Analysis

Many parameters affected the pressure-flow scouring process. A functional relationship between the maximum scour depth and independent variables associated with pressure-flow scour according to [15, 19] can be expressed as

$$y_s = f(y_a, y_b, L, B, b, b_{br}, h_s, h_g, V_a, V_b, u_*, d_{50}, \sigma_g, S_g, \rho, \nu, g) \quad (1)$$

where y_s is the maximum scour depth, f is the functional symbol, y_a is the approach flow depth, y_b is the flow depth under the bridge deck, L is the bridge length (contraction length = abutment length), B is the flume width, b is the width of the wall abutment, $b_{br} = (B - 2b)$ is the bridge width (contraction width), hg is the girder depth, h_s is the submerged height of the deck, V_a is the approach flow velocity, V_b is the flow velocity underneath the deck, u_* is the shear velocity, d_{50} is the median bed material size, σ_g is the geometric standard deviation, $S_g = (\rho_s/\rho)$ is the specific gravity of the bed materials, ρ_s is the density of the bed materials, ρ is the density of water, ν is the kinematic viscosity of water, and g is the gravitational acceleration (Figure 2). Using the Buckingham Pi theorem, the following dimensionless relationships are expressed as follows:

$$\frac{y_s}{y_a} = f\left(\frac{y_b}{y_a}, \frac{L}{y_a}, \frac{b_{br}}{B}, \frac{h_g}{y_a}, \frac{h_s}{y_a}, \frac{V_a}{V_b}, \frac{u_*}{V_b}, R, S_g, \sigma_g, F_a, \frac{d_{50}}{y_b}\right) \quad (2)$$

where F_a is the approach Froude number ($F_a = V_a/\sqrt{g y_a}$) and R is the approach Reynolds number ($R = V_a y_a/\nu$). The effect of the Reynolds number can be neglected, when the flow is fully turbulence (R > 10,000), [24]. The flume width and the girder depth were kept constant in all experiments (B = 60 cm and h_g = 1.5 cm, respectively). The terms h_s/y_a and V_a/V_b were dependent on the approach flow depth and the depth under the bridge deck ($h_s = y_a - y_b - h_g$). The term u_*/V_b is only dependent on the height under the bridge deck (bridge opening), and the parameter y_b/y_a included the same effect as that of u_*/V_b [15]. The densimetric Froude number ($F_a^* = V_a/\sqrt{g(S_g - 1)y_a}$) was used as three different bed materials were involved in this study, and the effect of the flow intensity V_a/V_c was included in F_a^* according to Carnacina et al. [25]. The relationship in Equation (2) can thus be simplified and arranged as follows:

$$\frac{y_s}{y_a} = f\left(\frac{y_b}{y_a}, \frac{L}{y_a}, \frac{b_{br}}{B}, \sigma_g, \frac{d_{50}}{y_b}, F_a^*\right) \quad (3)$$

3. Results and Discussion

A nonlinear regression analysis was applied to fit the independent variables given on the right-hand side of Equation (3) to the laboratory data using IBM SPSS (Statistical Package for Social Sciences) advanced statistics software for defining the constant coefficients that give the best fitting. The analysis produced an empirical equation for the combined vertical contraction due to the deck of the bridge and horizontal contraction due to the vertical wall abutments governed by clear water scour conditions as follows:

$$\frac{y_s}{y_a} = 1.55\left(\frac{y_b}{y_a}\right)^{-0.87}\left(\frac{L}{y_a}\right)^{-0.19}\left(\frac{b_{br}}{B}\right)^{-4.24}\left(\frac{d_{50}}{y_b}\right)^{-0.21}(\sigma_g)^{1.13}(F_a^*)^{1.62} \quad (4)$$

This relationship (Eq. 4) is valid for the considered range of parameters in this research ($0.313 \le y_b/y_a \le 0.85$, $3.33 \le L/y_a \le 10$, $0.733 \le b_{br}/B \le 0.917$, $0.009 \le d_{50}/y_b \le 0.074$, $1.198 \le \sigma_g \le 1.302$, $0.128 \le F_a^* \le 0.33$). The coefficient of determination (R^2) for Equation (4) was 0.92, and the adjusted $R^2 = 0.912$. This denotes that the degree of agreement between the parameters is reasonably good. B_{br}/B, F_a^*, σ_g, and y_b/y_a were the most significant variables in Equation (4) as $p < 0.001$ for these variables. Figure 3 depicts the observed scour depths against the estimated values for the pressure flow. The agreement between the observed and computed values revealed that Equation (4) could estimate the pressure-flow scour depth and could be applied as a preliminary design for bridges under pressure-flow conditions.

The reliability of the present laboratory data was examined using 35 data points to compute the relative maximum scour depth (y_s/y_a) using the earlier pressure-flow scour equations of Arneson and Abt [9], Umbrell et al. [3], Lyn [4], Guo et al. [11], HEC-18 Equation [2], Shan et al. [13], Melville [16], Kumcu [17], and Kocyigit and Karakurt [15] (Table 1). Moreover, Figure 3 plots the measured y_s/y_a for pressure-flow conditions and those calculated by the abovementioned models and Eq. (4). All the models except that of Kumcu [17] underpredicted the maximum scour depth for pressure-flow conditions, which is undesirable in engineering practice. Notably, the data of Arneson and Abt [9] and Umbrell et al. [3] gave many negative scour values, revealing unrealistic behaviors. The data of Kocyigit and Karakurt [15] also produced some negative values of scour depth. In this regard, Kocyigit and Karakurt [15] developed an empirical equation that involved the independent dimensionless parameter h_g/y_b. The actual girder depth (h_g) or number of girders was not examined in the current study. All negative scour values were eliminated and were not considered in the comparison. The computed negative scour values confirmed the conclusions of Lyn [4], where, as in the experiments of Arneson and Abt [9] and Umbrell et al. [3], an equilibrium scour state was not achieved.

A statistical analysis of the predictive errors for the tested models was performed. The statistical characteristics of the errors, including the average, minimum and maximum errors, variation coefficients of the errors, and root mean square error (RMSE) are listed in Table 4. The RMSE indicated that the worst performance during the testing was obtained from the model of Arneson and Abt [9]. The other prediction models [2, 3, 4, 11, 13, 15, 17] performed well with the current laboratory data. The computed RMSE for the model of HEC-18 Equation [2] as an error indicator was 0.390, the lowest RMSE among those of the tested models. This implies that this model performed better using the tested data set. The equations of Lyn [4], Guo et al. [11], Shan et al. [13], and Kocyigit and Karakurt [15] yielded roughly the same RMSE values.

Table 4. Error statistics for different models using current laboratory data sets.

Model/ Statistical Characteristics	Average Error	Minimum Error	Maximum Error	Variance	RMSE
Arneson and Abt [9]	0.522	−0.241	2.477	0.157	0.650
Umbrell et al. [3]	0.463	0.028	2.135	0.045	0.509
Lyn [4]	0.402	−0.017	2.112	0.047	0.455
Guo et al. [11]	0.357	−0.225	0.980	0.120	0.494
HEC-18 Equation [2]	0.280	−0.146	2.053	0.085	0.390
Shan et al. [13]	0.385	−0.041	2.190	0.051	0.445
Melville [16]	0.544	0.001	2.488	0.088	0.618
Kumcu [17]	-0.420	−0.919	1.347	0.082	0.506
Kocyigit and Karakurt [15]	0.430	0.166	1.773	0.015	0.447

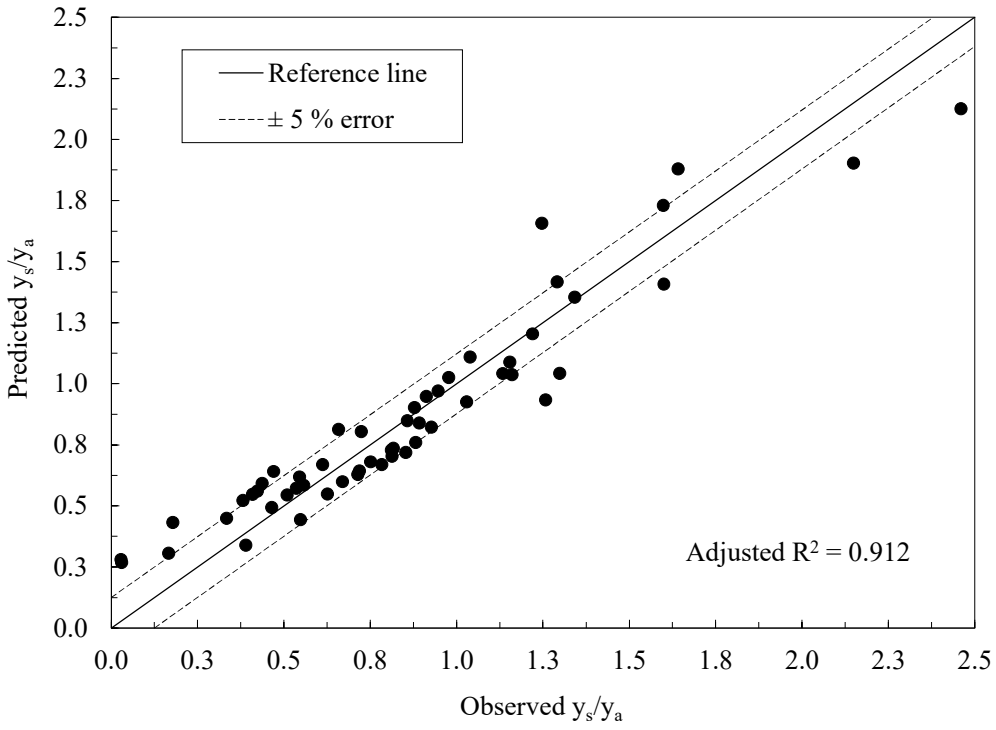

(**a**)

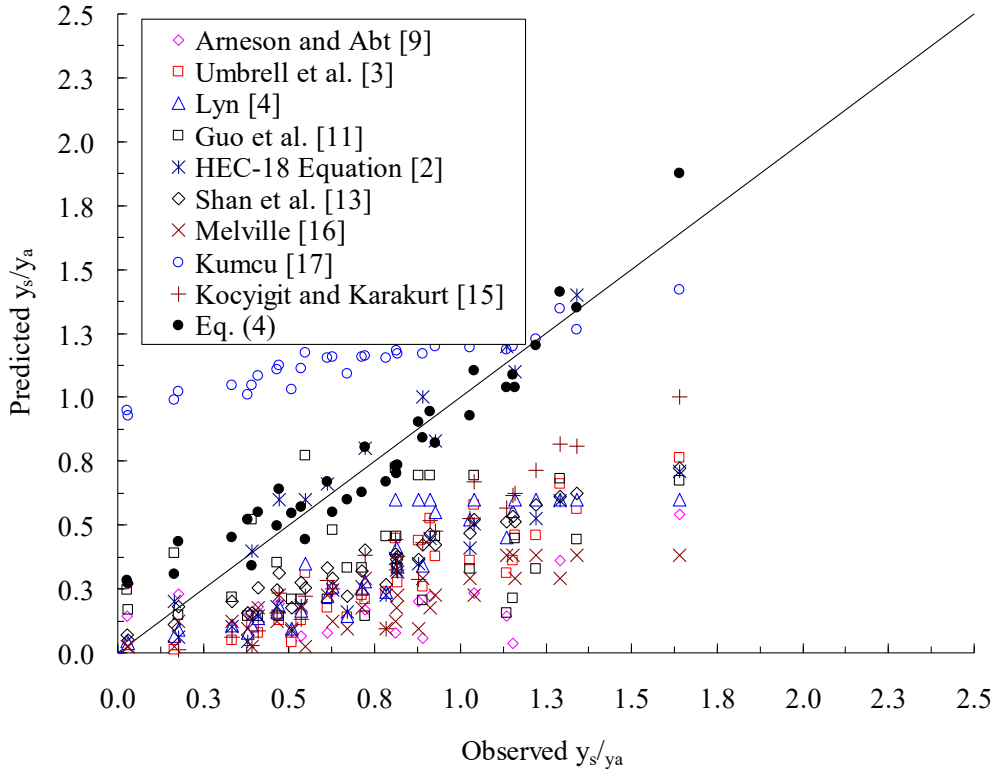

(**b**)

Figure 3. Observed relative maximum scour depth (y_s/y_a) versus those predicted: (**a**) using Equation (4); (**b**) using the literature equations, see Table (1).

3.1. Free Surface and Pressure-Flow Scour

To evaluate the effect of pressure-flow against atmospheric flow conditions, the laboratory data were used to present the relative maximum scour depth (y_s/y_a) at different relative bridge opening (y_b/y_a) for pressure-flow conditions and for the case of atmospheric flow conditions (y_b/y_a = 1.0) (Figure 4). The pressure-flow conditions produced a larger scour depth than that of the atmospheric flow conditions, which is consistent with Melville [16]. For the pressure and free surface flow conditions, the maximum scour depth increased when the densimetric Froude number increased. In addition, the relative scour depth increased as the relative bridge opening decreased and as the submergence ratios (h_s/y_a) increased ($h_s = y_a - h_g - y_b$). The maximum scour depth increased by up to about 77%, 73%, 69%, 58%, and 46% for range of the relative openings of y_b/y_a = 0.31~0.40, 0.51~0.60, 0.61~0.70, 0.71~0.80, and 0.76~0.85, respectively, compared with the maximum scour depth under atmospheric flow conditions. Decreasing the bridge openings increased the bed shear stress, which increased the scouring potential of flow. For the pressure-flow conditions, the maximum scour depth was 2.29 to 11.30 times larger than the atmospheric flow scour depending on the densimetric Froude number, the submergence ratios, and bridge openings. Abed [8] believed that the maximum scour depth increased by a factor ranging from 2.3 to 10, whereas Carnacina et al. [25] reported that the maximum scour depth increased by a factor of 2.52 times that under atmospheric flow conditions. It should be noted that these two previous investigations comprised both pressure-flow scour and pier scour. Guo et al. [11] defined the scour number $(y_s+y_b)/(y_b+h)$ where $h = (y_a-y_b)$ as similarity numbers to describe the bridge pressure-flow scour. The present laboratory data were employed to compute the scour numbers and are listed in Table 3. The computed scour numbers at same inundation Froude number ($F_i = V_a/\sqrt{g(y_a - y_b)}$), agree well with the analytical solution of Guo et al. [11].

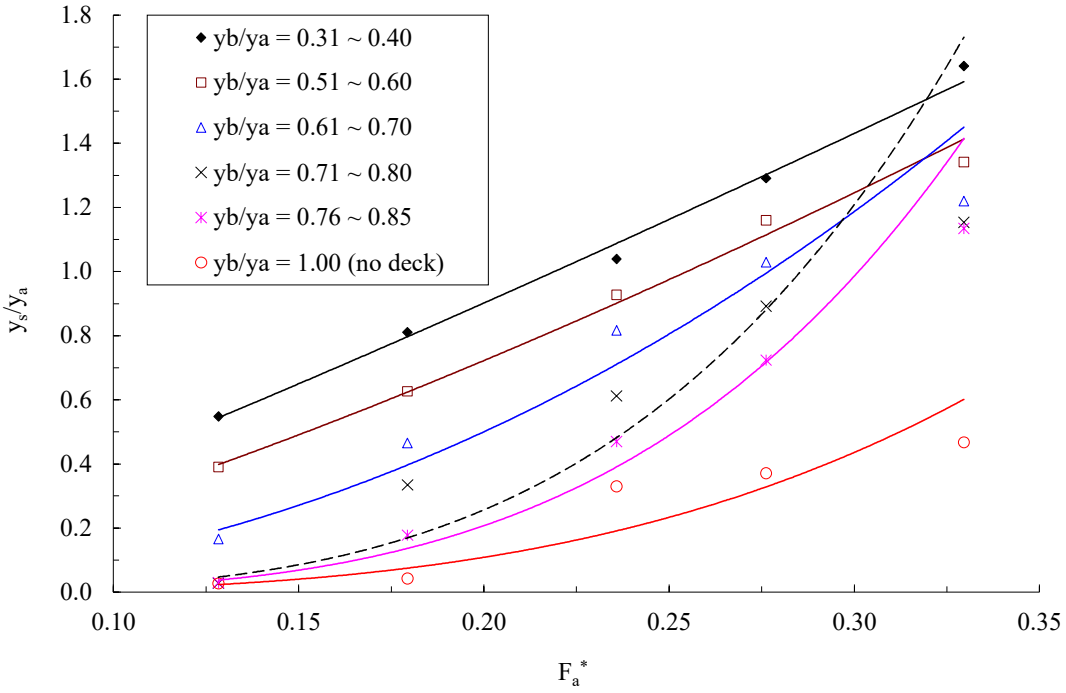

Figure 4. Relative maximum scour depth (y_s/y_a) versus the densimetric Froude number (F_a^*) for different relative bridge openings (y_b/y_a).

3.2. Water Surface Profile and Velocity Field

In all pressure-flow experiments, the downstream low chord of the bridge deck was found partially submerged. Thus, the bridge under pressure-flow conditions operates as an outlet orifice. The water surface level on the upstream side of the deck is higher than that on the downstream end as the deck acted as a flow barrier. During the tests, a dye injection was used and indicated that there were vortices on the upstream side of the deck extending toward the downstream part of the deck. A shear layer was formed at the lower side of the bridge deck, whereas vortices were formed between the two girders. Moreover, a reverse flow was observed just upstream and downstream of the deck. The movement of the shear layer to the free water surface on the downstream end of the bridge deck caused water surface fluctuations. The thickness of the shear layer and the strength of the vortices increased as the relative opening (y_b/y_a) decreased, and the approach densimetric Froude number increased. The flow observations under the pressure-flow conditions agreed with the flow descriptions of Picek et al. [26] and Lin et al. [12]. The measurements of the water surface profiles are depicted in Figure 5. According to this figure, the water surface elevation increased in the upstream face of the bridge deck and decreased just downstream of the deck (heading-up occurrence). This is the most important feature of the measured water surface profiles. The relative flow depth y/y_a increased gradually as the relative opening decreased. It was observed that the water surface upstream of the deck increased under atmospheric flow, which implied the effect of the two vertical wall abutments. The relative water surface in front of the deck increased by a factor of 11, 9, 6, 5, and 4 times the relative water surface in front of the deck under atmospheric flow conditions for y_b/y_a = 0.35, 0.55, 0.65, 0.75, and 0.80, respectively. The densimetric Froude number had a significant influence on the water surface profile under pressure-flow conditions as the heading-up was proportional to the velocity. The relative flow depth y/y_a increased as the relative bridge width (b_{br}/y_a) decreased. The relative bridge length L/y_a had a relatively small effect on the water surface profiles.

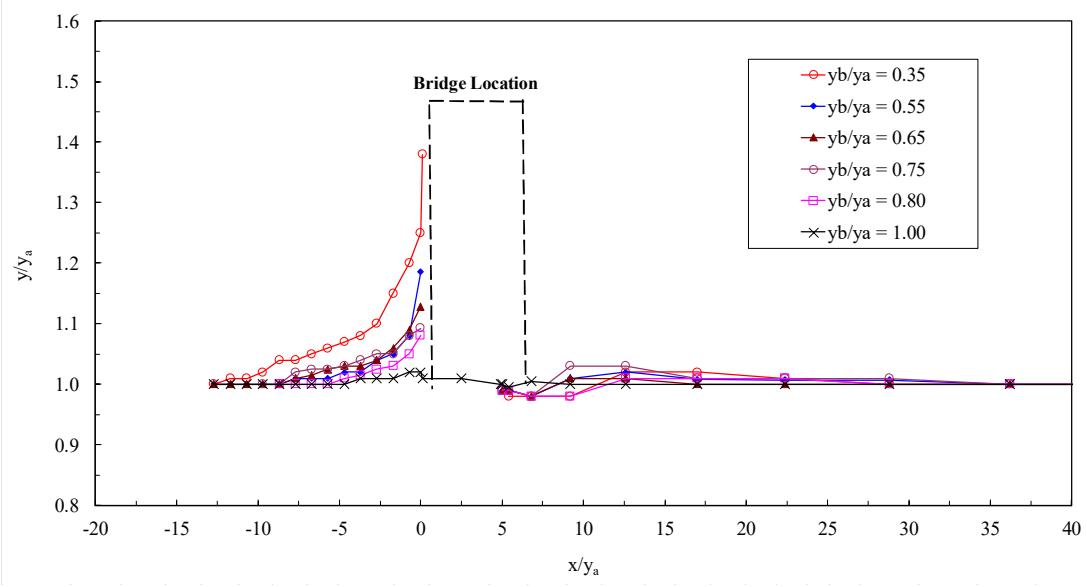

(**a**)

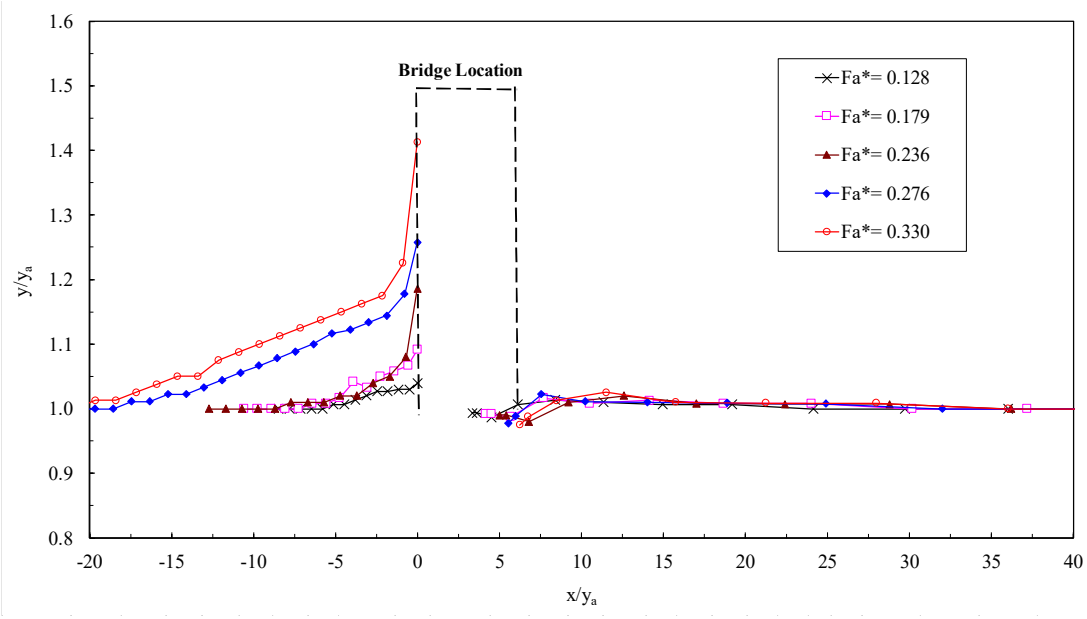
Bridge Location
Fa*= 0.128
Fa*= 0.179
Fa*= 0.236
Fa*= 0.276
Fa*= 0.330
y/ya
x/ya

(**b**)

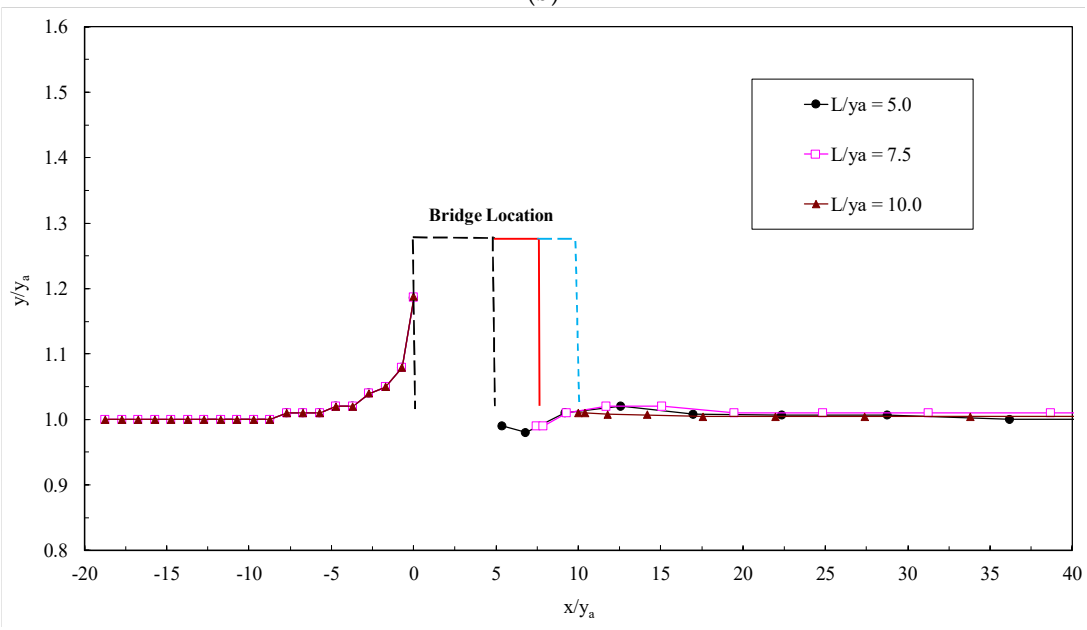
Bridge Location
L/ya = 5.0
L/ya = 7.5
L/ya = 10.0
y/ya
x/ya

(**c**)

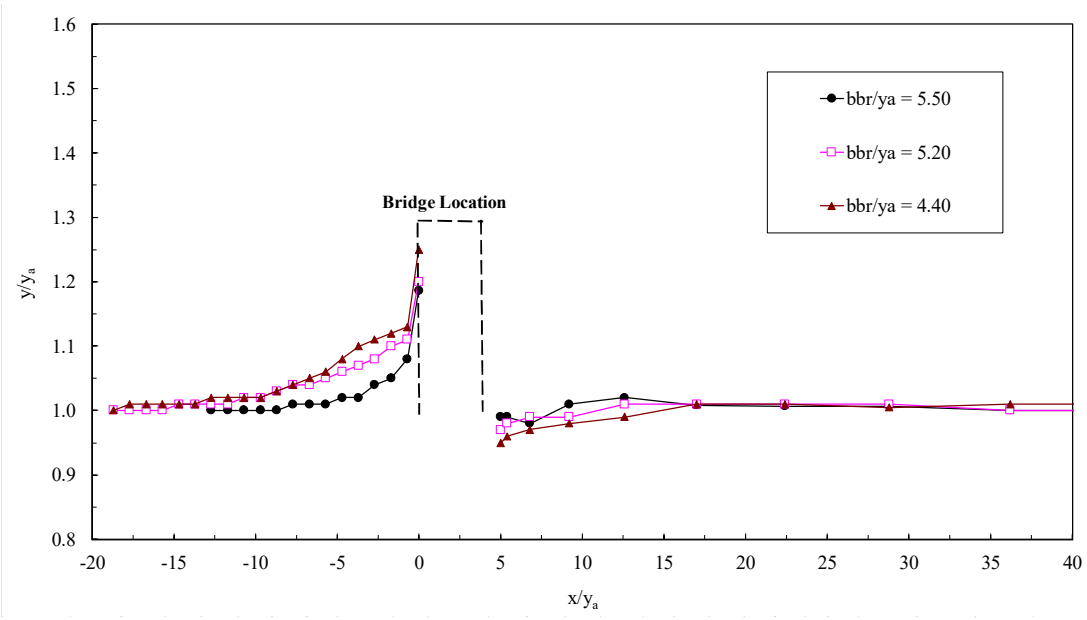

(**d**)

Figure 5. Relative flow depth y/y_a in the nondimensional streamwise distance x/y_a: (**a**) for different relative bridge openings y_b/y_a and $F_a^* = 0.236$; (**b**) for different densimetric Froude numbers and $y_b/y_a = 0.55$; (**c**) for different relative bridge lengths L/y_a and $y_b/y_a = 0.55$; and (**d**) for different relative bridge widths b_{br}/y_a and $y_b/y_a = 0.55$.

Seven vertical velocity profiles of dimensionless mean streamwise velocity (u/V_a) at dimensionless longitudinal distances (x/y_a) starting from the upstream to the downstream of the deck for different relative openings are plotted in Figure 6. Fifteen vertical points were measured for every vertical velocity profile along the centerline of the flume ($B/2$). The measured vertical velocity profile like that observed in open channels (logarithmic profile) was observed at nondimensional streamwise distances of $x/y_a = -7.0$). As the flow approached the bridge deck, the vertical velocity profile was affected near the water surface at $x/y_a = -5.0$. A small reverse flow near the free water surface was observed at $x/y_a = -5.0$ with $y_b/y_a = 0.35$. The velocity was negative or close to zero depending on the submergence ratios at just below the free surface at $x/y_a = -2.5$. This refers to the observed reverse flow near the free water surface and denotes the formation of the shear layer upstream of the bridge deck. Under the bridge deck ($x/y_a = 0.0$ to 5.0), vortices were observed, and the thickness of the shear layer increased under the bridge deck (Figure 6). The observed velocity profile under the bridge deck at $x/y_a = 2.5$ was similar to the velocity profile in pipe flow. The thickness of the shear layer increased as the relative opening y_b/y_a decreased. The vertical velocity distribution just downstream of the deck was similar to that of horizontal jet flow. After the flow passed through the bridge deck ($x/y_a = 6.0$), negative velocities were observed toward the free surface as the shear layer moved toward the free surface, and this generated vortices at the water surface. Downstream of the bridge deck at $x/y_a = 6.0$, the development of a boundary layer flow was dominant near the bed. The near-bed velocity gradients were clearly higher than that of $x/y_a = 2.5$. The gradient was almost vertical. This indicated that shear stresses were generated under the bridge deck. For each vertical profile, the maximum velocity was found to be almost in the middle of the vertical profile. The observations of the velocity field in pressure-flow scour agrees well with the depictions by [12,27,28]. It is worth mentioning that the pressure flow accelerated the flow near the abutments, resulting in scour holes in front and alongside them.

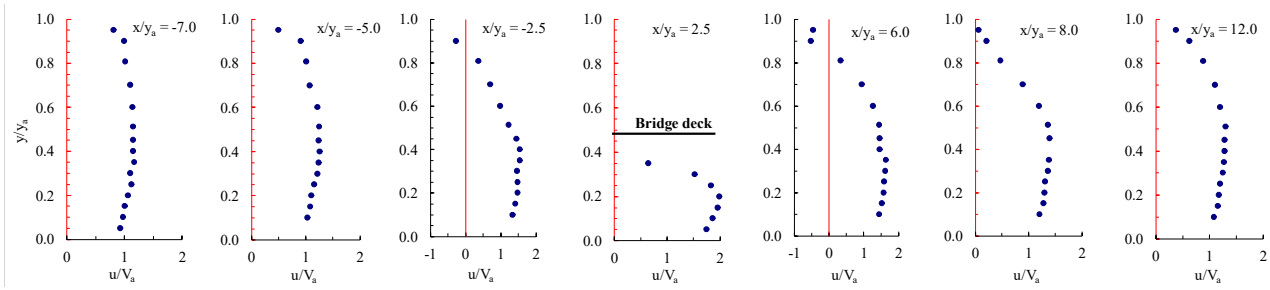
x/y_a = -7.0
x/y_a = -5.0
x/y_a = -2.5
x/y_a = 2.5
Bridge deck
x/y_a = 6.0
x/y_a = 8.0
x/y_a = 12.0
y/y_a
u/V_a

(**a**)

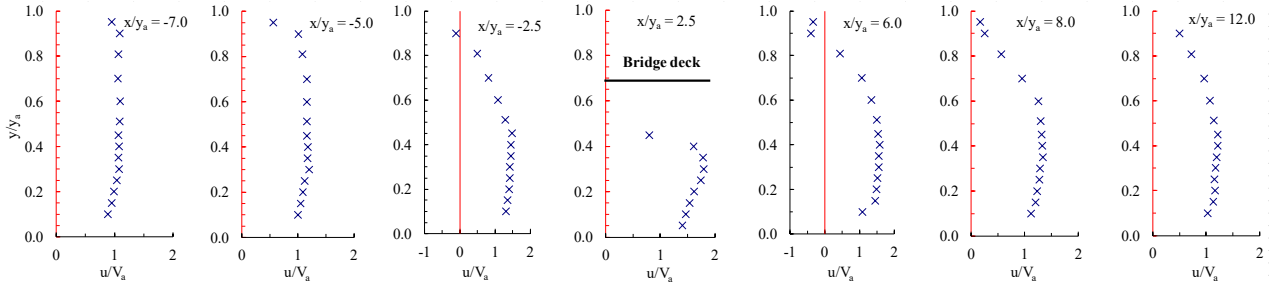
x/y_a = -7.0
x/y_a = -5.0
x/y_a = -2.5
x/y_a = 2.5
Bridge deck
x/y_a = 6.0
x/y_a = 8.0
x/y_a = 12.0
y/y_a
u/V_a

(**b**)

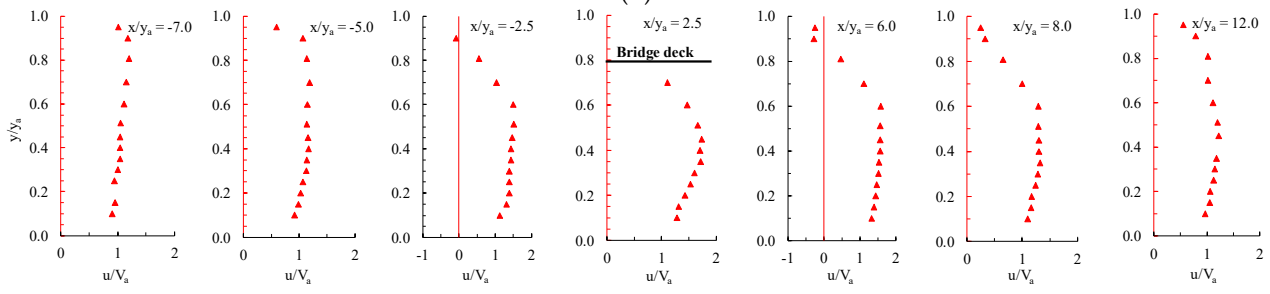
x/y_a = -7.0
x/y_a = -5.0
x/y_a = -2.5
x/y_a = 2.5
Bridge deck
x/y_a = 6.0
x/y_a = 8.0
x/y_a = 12.0
y/y_a
u/V_a

(**c**)

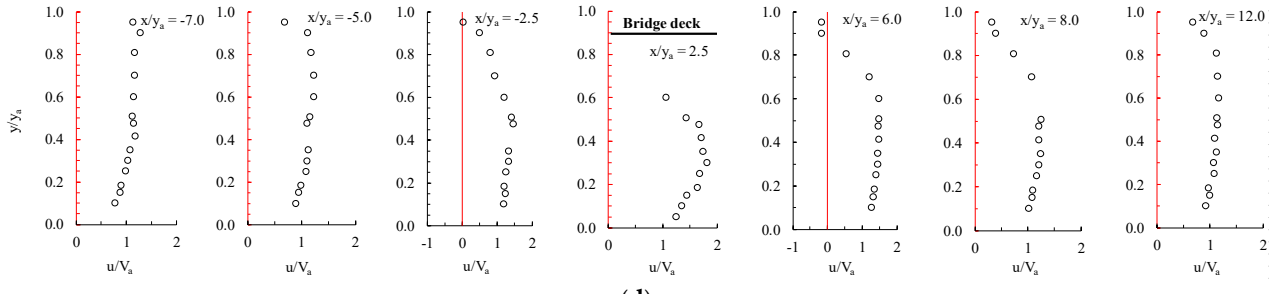
x/y_a = -7.0
x/y_a = -5.0
x/y_a = -2.5
Bridge deck
x/y_a = 2.5
x/y_a = 6.0
x/y_a = 8.0
x/y_a = 12.0
y/y_a
u/V_a

(**d**)

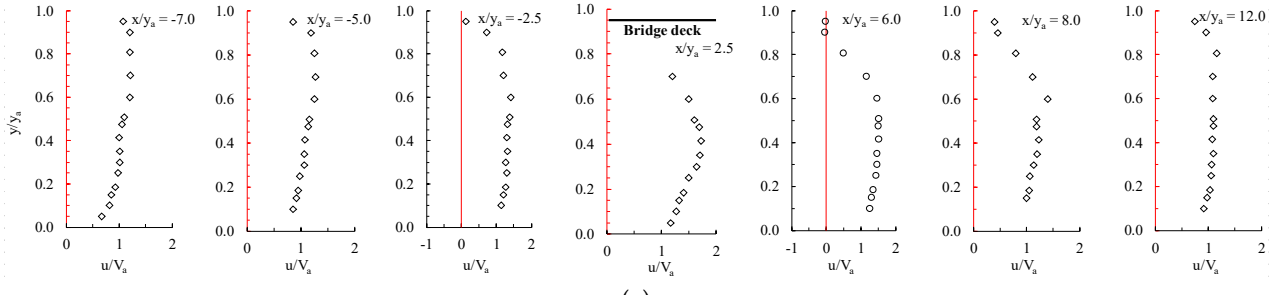
x/y_a = -7.0
x/y_a = -5.0
x/y_a = -2.5
Bridge deck
x/y_a = 2.5
x/y_a = 6.0
x/y_a = 8.0
x/y_a = 12.0
y/y_a
u/V_a

(**e**)

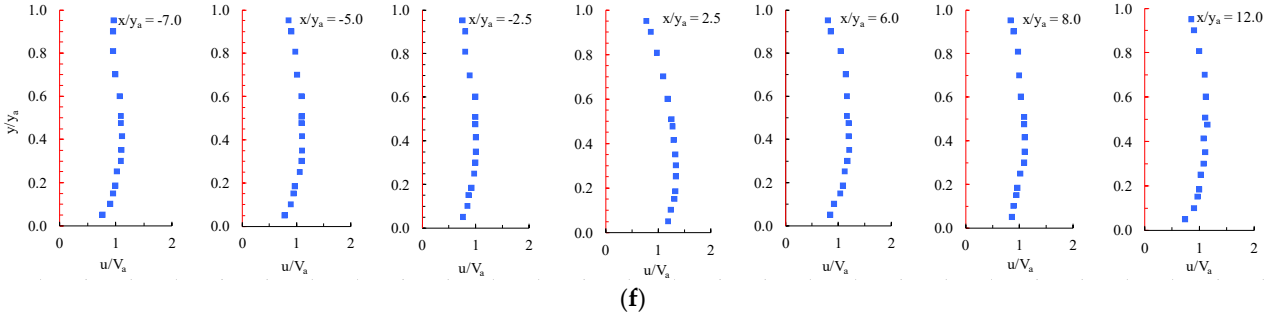

Figure 6. Vertical distributions of the nondimensional mean streamwise velocity u/V_a at centerline of the channel and at different nondimensional streamwise distances x/y_a, $F_a^* = 0.236$ and at: (**a**) $y_b/y_a = 0.35$; (**b**) $y_b/y_a = 0.55$; (**c**) $y_b/y_a = 0.65$; (**d**) $y_b/y_a = 0.75$; (**e**) $y_b/y_a = 0.80$; and (**f**) $y_b/y_a = 1.00$ (no deck).

3.3. Pressure-Flow Scour Profile

The observed scour first developed in the central part of the flume upstream of the bridge deck and then progressed laterally. A scour was also observed in front of the abutments. Figure 7 shows the centerline profiles of the scour hole for the pressure and atmospheric flow conditions at $F_a^* = 0.236$ and $d_{50} = 1.093$. According to Figure 7, the observed location of the maximum scour depth was below the deck and close to its downstream side. This was because the flow was accelerated in the streamwise direction; the maximum velocity was observed under the bridge deck, which was greater than the critical velocity of the bed material particles. According to Hahn and Lyn [29], the observed location of the maximum scour depth was after the downstream end of the bridge deck. This study agrees well with the measurements of Guo et al. [23] and Shan et al. [13] but is contrary to Hahn and Lyn [29]. A scour hole was observed under the free surface flow conditions in the no-deck case ($h_s/y_a = 0.0$). This indicated that the maximum scour depth in the present experiments resulted from both pressure-flow scour and abutment scour. The maximum scour depth under the pressure-flow conditions was notably larger than those under the free surface flow conditions, which corresponded to the velocity distribution. The upstream slope of the scour hole was steeper than the downstream slope, which implied that the equilibrium scour depth was not sustained. The maximum scour depth and the upstream and downstream scour slopes increased when the relative openings decreased as scour particles were deposited at the downstream side. The increase in the relative openings decreased the bed shear, which increased the scouring potential of flow. The relative openings did not affect the location of the maximum scour depth. Although the maximum scour depth marginally decreased as the bridge length increased, the scour hole length in the streamwise direction increased as the bridge length increased. This revealed that underneath the longer deck, the velocity distribution becomes uniform along the bridge deck length and the bed elevation redistributes during the test to produce a longer and superficial scour hole. The maximum scour depth significantly increased as the bridge width decreased under pressure-flow conditions.

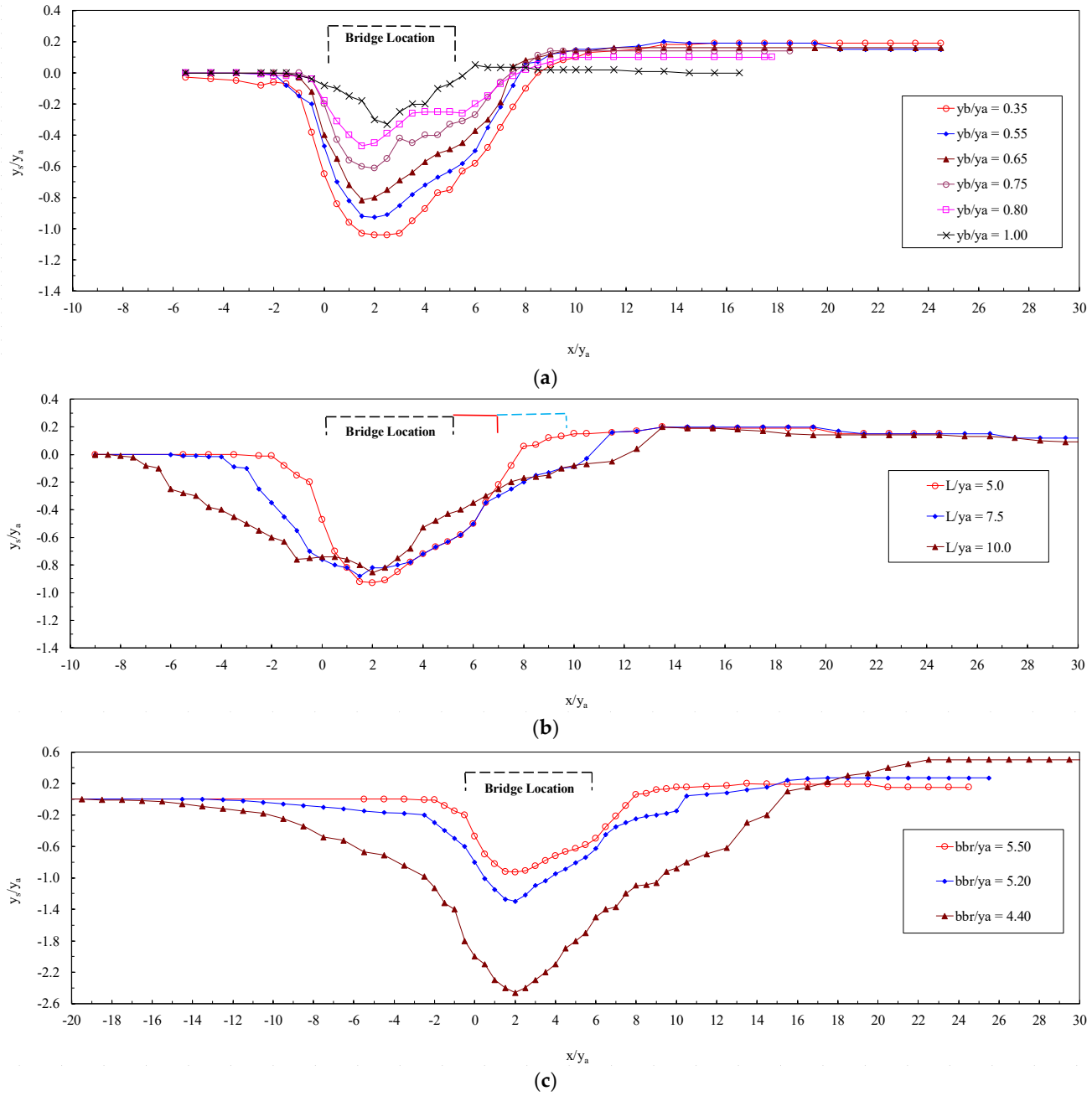

Figure 7. Relative scour depth y_s/y_a in the nondimensional streamwise distance x/y_a for $F_a^* = 0.236$ and for: (**a**) different relative bridge opening y_b/y_a; (**b**) different relative bridge lengths L/y_a and $y_b/y_a = 0.55$; and (**c**) different relative bridge widths (b_{br}/y_a) and $y_b/y_a = 0.55$.

Three different types of sand with median diameters (d_{50}) of 1.093, 1.469, and 2.575 mm were tested to explore the effects of the bed material size on the maximum scour depth (y_s). The relative maximum scour depth y_s/y_a with the relative bridge opening (y_b/y_a) for different relative median diameters of bed materials (d_{50}/y_b) is depicted in Figure 8. It was found that for pressure-flow, as the bridge opening (y_b) increased, the maximum scour depth decreased by up to about 54.8% for $d_{50} = 1.093$ mm, 55.2% for $d_{50} = 1.469$ mm, and 56.6% for $d_{50} = 2.575$ mm. It was observed that the maximum scour depth increased when finer bed materials were tested. This is because increasing the bed material

size increased the critical velocity of shields and correspondingly decreased the scour depth.

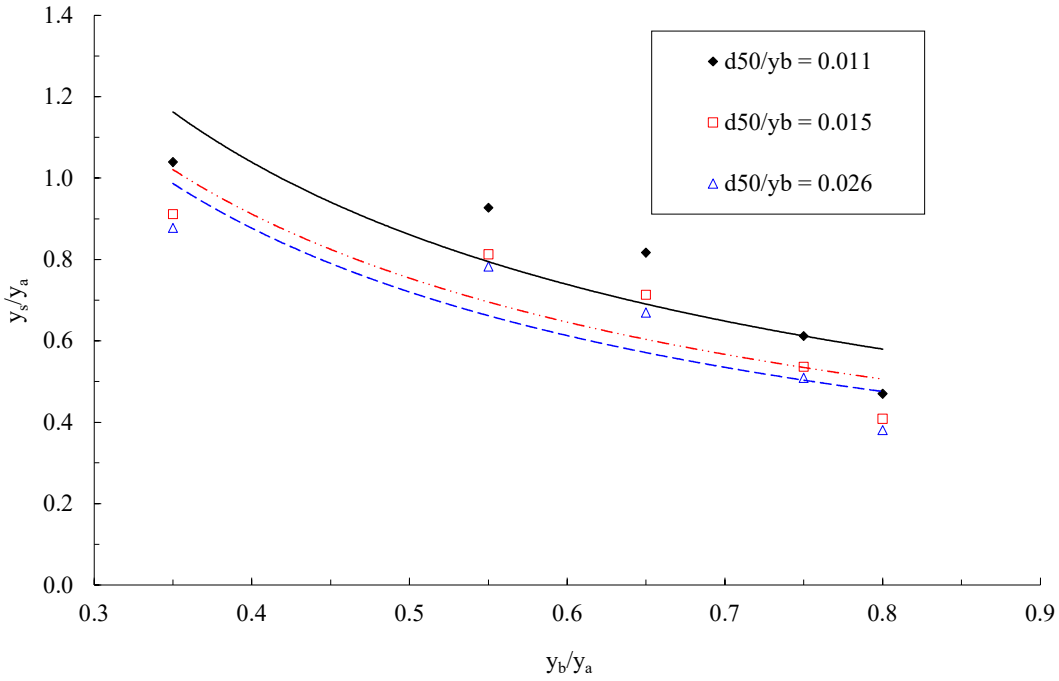

Figure 8. Relative scour depth y_s/y_a with the relative bridge opening for different relative median bed materials (d_{50}/y_b).

3.4. Effects of the Bridge Length and Width

Majid and Tripathi [7] reported that the effects of the bridge length (L) (length of contraction) and bridge width (b_{br}) (contraction width) on the scour depth under pressure-flow conditions have not been investigated in any study.

The current research examined three bridge lengths: L = 50, 75, and 100 cm (Figure 9). It was observed that the scour depth decreased as the bridge opening (y_b) increased. When the relative bridge length was increased from 5 to 7.5 and from 7.5 to 10, the scour depth decreased by up to about 7.4% and 2.3%, respectively. The maximum scour depth slightly decreased when a longer bridge was tested. This was because an increase in the bridge length redistributed the velocity in the streamwise direction; thus, the velocity field underneath the bridge deck became more symmetric during the test to produce a shallower scour hole. Figure 9 plots the relative scour depth y_s/y_a with the relative bridge opening y_b/y_a for different relative bridge widths (b_{br}/y_a). Similar to the contraction length, as the bridge opening height decreased, the scour depth increased. As the relative bridge width decreased from 5.5 to 5.2 and from 5.2 to 4.4, the maximum scour depth increased by up to about 45.6% and 81.2%, respectively. The scour depth significantly increased when the bridge width decreased. This indicates that as the bridge width decreased, the velocity field underneath the deck is notably increased; consequently, the shear stress increased. The scour depth is a combined scour of both the contraction width and the pressure-flow conditions. New experimental data are needed to further evaluate the contraction length and width of the pressure-flow scour and fill the gap in the literature.

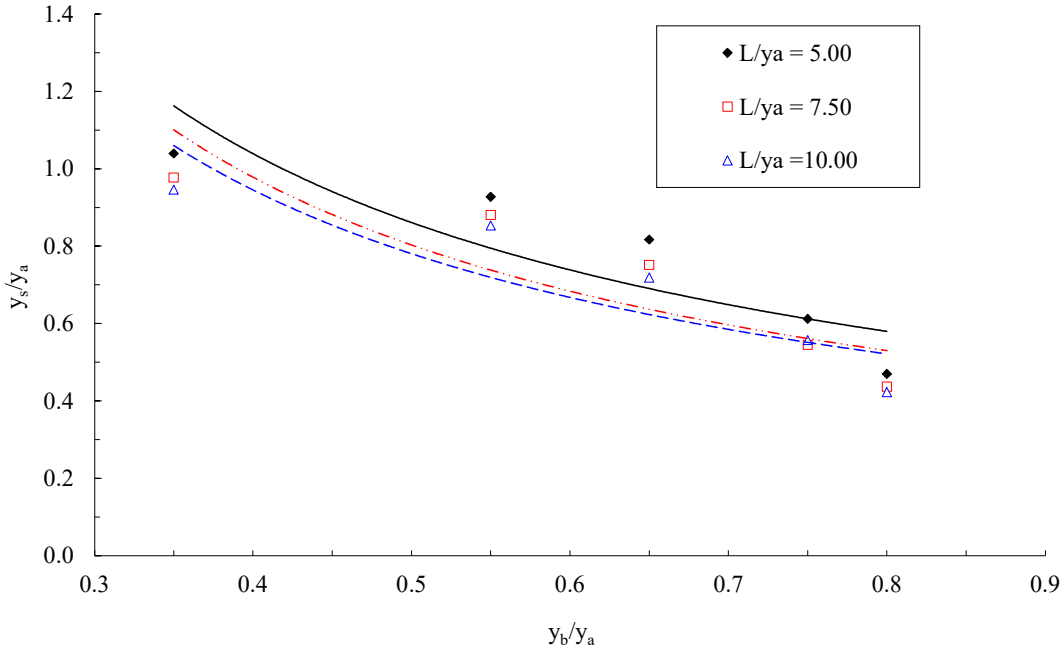

(**a**)

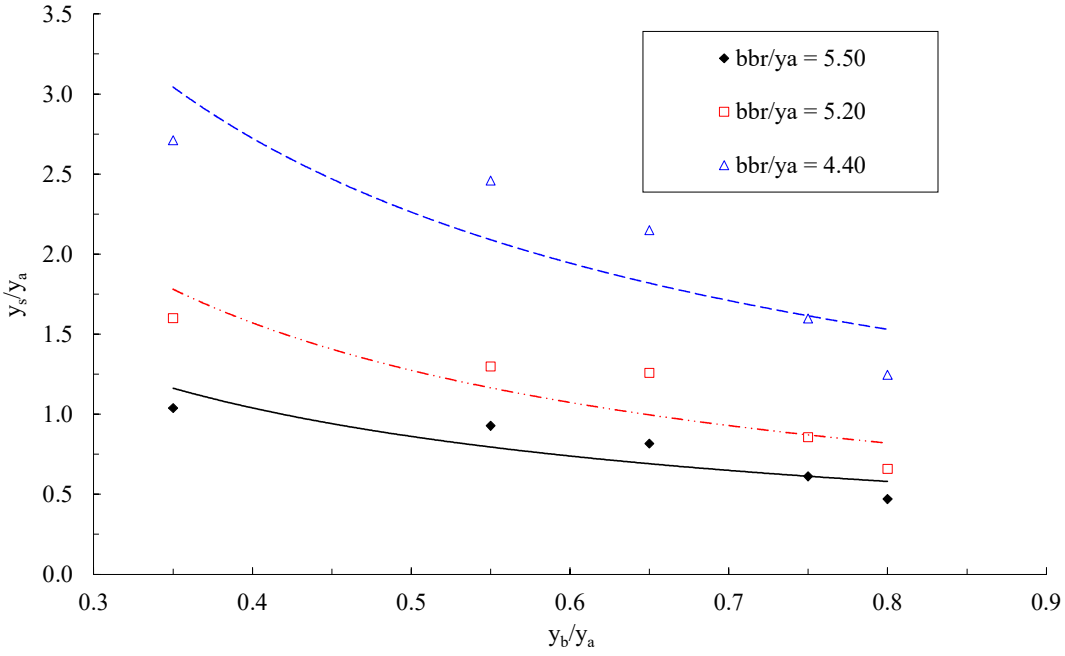

(**b**)

Figure 9. Relative scour depth y_s/y_a with the relative bridge opening y_b/y_a for (**a**) different relative bridge lengths (L/y_a) and (**b**) different relative bridge widths (b_{br}/y_a).

4. Conclusions

This study explored the scour depth beneath a bridge deck without piers for atmospheric and pressure flows under clear water conditions in the presence of two vertical wall abutments. Through the experiments, the effects of the flow depth, bed material size, contraction length, contraction width, and bridge opening on the maximum scour depth were examined in both flow conditions. A dimensionless relationship was deduced to

predict the maximum scour depth due to the vertical deck and horizontal abutment contractions. Statistical analyses were applied to assess the agreement of the laboratory data with previously published models. The present laboratory equation can be employed in the initial design of bridges under pressure-flow conditions. The experimental data were used to analyze the predictive errors of the previous models. The results showcased that the HEC-18 Equation performed better than the other tested models and gave the lowest RMSE. Under the pressure-flow conditions, the maximum scour depth increased by a factor between 2.15 and 9.81 times that under the atmospheric flow conditions depending on the densimetric Froude number and bridge openings. The most important features of the measured water surface profiles were of the water surface elevation increase on the upstream side of the bridge deck, and the decrease just downstream of the deck. As the bridge opening increased, the maximum scour depth decreased, while it increased in the presence of finer bed materials. When the relative bridge length was increased from 5 to 7.5 and from 7.5 to 10, the maximum scour depth decreased by up to about 7.4% and 2.3%, respectively. Decreasing the relative bridge width from 5.5 to 5.2 and 5.2 to 4.4, the maximum scour depth increased by up to about 45.6% and 81.2%, respectively. Scouring at bridge abutments is the major cause of bridge collapses worldwide. Therefore, the next steps in this research would be to expand the evaluation on the contraction lengths and widths of pressure-flow scours by conducting more experimental assessments and enriching the literature on this less researched aspect. This further evaluation would contribute to a better database for computing the scour risk of bridge foundations which is key for a correct management approach and allocation of resources for maintenance and scour mitigation works.

Author Contributions: Conceptualization, F.S.A.; methodology, F.S.A.; experiments, F.S.A.; formal analysis, F.S.A., W.F. and I.M.M.; investigation, I.G.S., A.A. and A.I.; data curation, F.S.A. and W.F.; writing—original draft preparation, F.S.A., I.G.S. and A.A.; writing—review and editing, F.S.A., I.G.S. and A.A. All authors have read and agreed to the published version of the manuscript.

Funding: No funding was received to assist with the preparation of this manuscript.

Data Availability Statement: The data are available from the first author upon reasonable request.
Acknowledgments: The authors express their sincere thanks to their colleagues at the Hydraulics Laboratory of the Faculty of Engineering, Menoufia University, Egypt, for facilitating the experimental work.

Conflicts of Interest: The authors have declared that no competing interests exist.

References

1. Gaudio, R.; Tafarojnoruz, A.; Calomino, F. Combined flowaltering countermeasures against bridge pier scour. *J. Hydraul. Res.* **2012**, *50*, 35–43. https://doi.org/10.1080/00221686.2011.649548.
2. Arneson, L.A.; Zevenbergen, L.; Lagasse, P.; Clopper, P. *Evaluating Scour at Bridges*; Report No. FHWA-HIF-12-003; USDOT, National Highway Institute (US): Washington, DC, USA, 2012.
3. Umbrell, E.R.; Young, G.; Stein, S.; Jones, J. Clearwater contraction scour under bridges in pressure flow. *J. Hydraul. Eng.* **1998**, *124*, 236–240. https://doi.org/10.1061/(ASCE)0733-9429(1998)124:2(236).
4. Lyn, D.A. Pressure-flow scour: A reexamination of the HEC-18 equation. *J. Hydraul. Eng.* **2008**, *134*, 1015–1020. https://doi.org/10.1061/(ASCE)0733-9429(2008)134:7(1015).
5. Richardson, E.V.; Harrison, L.; Richardson, J.; Davis, S. *Evaluating Scour at Bridges HEC 18: Hydraulic Engineering Circular*, 2nd ed.; Federal Highway Administration: Washington, DC, USA, 1993; pp. 5–53.
6. Carnacina, I.; Leonardi, N.; Pagliara, S. Characteristics of flow structure around cylindrical bridge piers in pressure-flow conditions. *Water* **2019**, *11*, 2240. https://doi.org/10.3390/w11112240.
7. Majid, S.A.; Tripathi, S. Pressure-flow scour due to vertical contraction: A review. *J. Hydraul. Eng.* **2021**, *147*, 03121002. https://doi.org/10.1061/(ASCE)HY.1943-7900.0001943.
8. Abed, L.M. Local Scour around Bridge Piers in Pressure Flow. Ph.D. Dissertation, Department of Civil Engineering, Colorado State University: Fort Collins, CO, USA, 1991; pp. 43–47, 61–63.
9. Arneson, L.A.; Abt, S.R. Vertical contraction scour at bridges with water flowing under pressure conditions. *Transp. Res. Rec.* **1998**, *1647*, 10–17. https://doi.org/10.3141/1647-02.

10. Arneson, L.A. The Effect of Pressure-Flow on Local Scour in Bridge Openings. Ph.D. Dissertation, Department of Civil Engineering, Colorado State University: Fort Collins, CO, USA, 1997.
11. Guo, J.; Kerenyi, K.; Pagan-Ortiz, J. *Bridge Pressure Flow Scour for Clear Water Conditions*; Report No. FHWA-HRT-09-041; Turner-Fairbank Highway Research Center, FHWA: McLean, VA, USA, 2009; pp. 24–29.
12. Lin, C.; Kao, M.J.; Hsieh, S.C.; Lo, L.F.; Raikar, R.V. On the flow structures under a partially inundated bridge deck. *J. Mech.* **2012**, *28*, 191–207.
13. Shan, H.; Bojanowski, C.; Xie, Z; Suaznabar, O.; Lottes, S.; Shen, J.; Kerenyi, K. *Submerged Flow Bridge Scour under Clear Water Conditions*; Publication No. FHWA-HRT-12-034; Federal Highway Administration: Washington, DC, USA, 2012.
14. Dankoo, A.; Yonesi, H.; Torabipoudeh, H.; Saneie, M. The effect of pressure flow conditions on bridge pier scour in compound open channels with vegetation. *J. Hydraul. Iran. Hydraul. Assoc.* **2022**, *17*, 89–103.
15. Kocyigit, M.B.; Karakurt, O. Pressure flow and weir scour beneath a bridge deck. *Can. J. Civ. Eng.* **2019**, *46*, 534–543. https://doi.org/10.1139/cjce-2017-0469.
16. Melville, B.W. Scour at various hydraulic structures: Sluice gates, submerged bridges, low weirs. *Aust. J. Water Resour.* 2014, 18, 101–117. https://doi.org/10.1080/13241583.2014.11465444.
17. Kumcu, S.Y. Steady and unsteady pressure scour under bridges at clear-water conditions. *Can. J. Civ. Eng.* **2016**, *43*, 334–342. https://doi.org/10.1139/cjce-2015-0385.
18. Dey, S.; Raikar, R.V.; Roy, A. Scour at submerged cylindrical obstacles under steady flow. *J. Hydraul. Eng.* **2008**, *134*, 105–109.
19. Raudkivi, A.J.; Ettema, R. Scour at cylindrical bridge piers in armored beds. *J. Hydraul. Eng.* **1985**, *111*, 713–731. https://doi.org/10.1061/(ASCE)0733-9429(1985)111:4(713).
20. Helal, E. Experimental evaluation of changes in channel bed morphology due to a defective pressure flow pipe. *J. Irrig. Drain. Eng.* **2019**, *145*, 04019022. https://doi.org/10.1061/(ASCE)IR.1943-4774.0001418.
21. Neill, C.R. *Guide to Bridge Hydraulics*; University of Toronto Press: Toronto, ON, Canada, 1973.
22. Melville, B.W. The physics of local scour at bridge piers. In Proceedings of the 4th International Conference on Scour and Erosion (ICSE-4), Tokyo, Japan, 4–8 November 2008; Japanese Geotechnical Society: Tokyo, Japan, 2008; pp. 28–40.
23. Guo, J.; Kerenyi, K.; Pagan-Ortiz, J.; Flora, K. Bridge pressure flow scour at clear water threshold condition. *Trans. Tianjin Univ.* **2009**, *15*, 79–94. https://doi.org/10.1007/s12209-009-0016-3.
24. Henderson, F.M. *Open Channel Flow*; The Macmillan Company: New York, NY, USA, 1966; p. 93.
25. Carnacina, I.; Pagliara, S.; Leonardi, N. Bridge pier scour under pressure flow conditions. *River Res. Appl.* **2019**, *35*, 844–854. https://doi.org/10.1002/rra.3451.
26. Picek, T.; Havlik, A.; Mattas, D.; Mares, K. Hydraulic calculation of bridges at high water stages. *J. Hydraul. Res.* **2007**, *45*, 400–406.
27. Hahn, E. Clear-Water Scour at Vertically or Laterally Contracted Bridge Sections. M.Sc. Dissertation, School of Civil Engineering, Purdue University, West Lafayette, IN, USA, 2005.
28. Yoon, K.S.; Lee, S.; Hong, S. Time-averaged turbulent velocity flow field through the various bridge contractions during large flooding. *Water* **2019**, *11*, 143. https://doi.org/10.3390/w11010143.
29. Hahn, E.M.; Lyn, D. Anomalous contraction scour? Vertical contraction case. *J. Hydraul. Eng.* **2010**, *136*, 137–141. https://doi.org/10.1061/(ASCE)0733-429(2010)136:2(137).